Commun. Math. Phys. 91, 103–116 (1983)

Communications in
Mathematical
Physics
© Springer-Verlag 1983

The Instability of Fronts in a Porous Medium*

Alexandre Joel Chorin**

Department of Mathematics, University of California, Berkeley, CA 94720, USA

Abstract. We use a random choice numerical method to analyze the instability of a front separating two fluids in a porous medium. We observe a linear instability and a catastrophic finite amplitude instability. A qualitative analogy with problems involving a transition to turbulence is pointed out.

Introduction

The goal of this paper is to present an analysis of the onset of instability in a front separating two fluids in a porous medium. The analysis will be based on Glimm's (random choice) numerical method. The front is known to be unstable for sufficiently large values of a parameter μ, the viscosity ratio. We shall show that there exist two kinds of instability: for $\mu \geqq \mu_0 = 3$, small perturbations that are spatially smooth will grow slowly: for $\mu \geqq \mu_1 < \mu_0$, perturbations of large enough amplitude grow catastrophically. The two types of instability can interact.

The results and the numerical method are of practical significance in problems of oil flow and resevoir engineering. A random choice method [13, 3, 4] has been previously applied to such problems by Concus et al. [1, 10], Glimm et al. [14, 15], and Lotstedt [19]. Our method differs from earlier work in several respects, the most important of which is the fact that we keep some two dimensional information in order to reduce the possibility that one dimensional sweeps misinterpret the nature of waves moving diagonally across the grid. The possibility of large errors in this situation has been pointed out by Crandall and Majda [11, 12] and by Colella [9]. We do not track fronts.

The results regarding the different kinds of instability resemble strongly other phenomena previously observed in hydrodynamics (see e.g. [5, 7, 22]). We have a

* This work was supported by the Director, Office of Energy Research, Office of Basic Energy Sciences, Engineering, Mathematical, and Geosciences Division of the U. S. Department of Energy, under Contract DE-AC03-76SF00098, and in part by the Office of Naval Research, under Contract N00014-76-C-0316

** The work was performed while the author was a Miller Research Professor at the University of California at Berkeley

continuum of unstable modes which can combine strongly to generate phenomena reminiscent of turbulence and intermittency. The present calculation may be helpful in explaining the gap between linearized stability theory and experiment in more difficult problems. These questions are discussed in the concluding section of the paper.

The Equations of Motion, the Riemann Problem, and Linearized Stability Theory

The incompressible flow of two immiscible fluids in a porous medium can be described by the following equations (see [24, 16, 21]):

$$s_t + \mathbf{u} \cdot \nabla f(s) = 0, \tag{1a}$$

$$\nabla \cdot \mathbf{u} = 0, \tag{1b}$$

$$\mathbf{u} = -\lambda(s) \nabla p, \tag{1c}$$

where s is the saturation of one of the fluids (which we shall think of as being "water"), t is the time, $\mathbf{x} = (x, y)$ is the spatial coordinate, $\mathbf{u} = (u, v)$ is the velocity, p is the pressure, λ is the total mobility, and f is the fractional flow function (for explanations of those terms see [24]). Equation (1a) is known as the Buckley-Leverett equation, (1b) expresses incompressibility, and (1c) is Darcy's law. We shall pick

$$\lambda(s) = s^2 + (1-s)^2/\mu, \tag{2a}$$

$$f(s) = s^2/\lambda(s), \tag{2b}$$

where μ is the viscosity ratio between the two fluids. (We shall think of the one which is not "water" as being "oil.") These choices correspond to immiscible flow. Note that f is not a convex function of s.

We shall be solving these equations in the square $0 \leqq x \leqq 1$, $0 \leqq y \leqq 1$, subject to the boundary conditions:

$$\begin{aligned} &\frac{\partial s}{\partial x} = 0, \frac{\partial p}{\partial x} = 0 \quad \text{on} \quad x = 0, 1, \\ &\frac{\partial s}{\partial y} = 0, p = 1 \quad \text{on} \quad y = 0, \\ &\frac{\partial s}{\partial y} = 0, p = 0 \quad \text{on} \quad y = 1, \end{aligned} \tag{3}$$

and a variety of initial conditions $s(x, y, 0)$.

The solutions of Eqs. (1) develop discontinuities, and we assume that discontinuities in two space dimensions satisfy jump conditions identical to those which arise in the scalar problem

$$s_t + u f_x = 0, f = f(s), \tag{4}$$

where x denotes the variable normal to the discontinuity. We shall now summarize some facts about Eq. (4); a detailed presentation is available in [10].

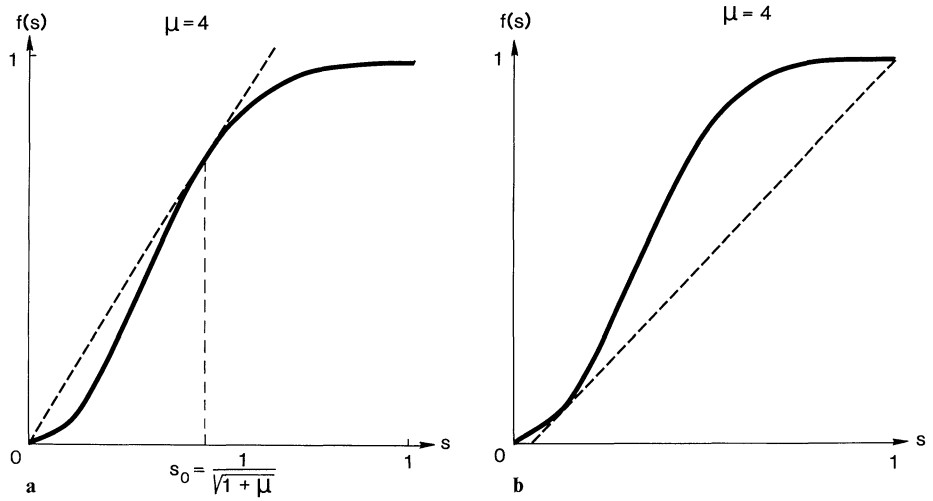

Fig. 1a and b. Convex and concave hulls of f

Let $u \equiv 1$ in Eq. (4). Let s_l, s_r be the values of s to the left and to the right of a jump discontinuity. The solution of (4) is unique and depends continuously on the data only if the jump in s satisfies Oleinik's condition (E):

$$\frac{f(s_r)-f(s)}{s_r-s} \leqq \frac{f(s_r)-f(s_l)}{s_r-s_l} \tag{E}$$

for all s between s_l and s_r. (For an elementary discussion, see [8].)

Consider the Riemann problem for Eq. (4), $u \equiv 1$, i.e., Eq. (4) subject to the initial data

$$s = \begin{cases} s_l & \text{for} \quad x<0 \\ s_r & \text{for} \quad x>0. \end{cases}$$

The states s_l, s_r will be connected by either a shock, or a rarefaction wave, or a combined shock and rarefaction. All shocks must obey condition (E), which determines uniquely the allowed connecting waves.

If the chord connecting the points $(s_l, f(s_l))$ and $(s_r, f(s_r))$ in the (s, f) plane nowhere intersects the graph of f, then if $a(s_l) > a(s_r)$, $a \equiv \frac{df}{ds}$, the connecting wave is a shock with speed $\frac{dx}{dt} = (f(s_r)-f(s_l))/(s_r-s_l)$: if, on the other hand, $a(s_l) \leqq a(s_r)$, the connecting wave is a rarefaction.

If the chord connecting $(s_l, f(s_l))$ and $(s_r, f(s_r))$ does intersect the graph of f, which can happen since f is not convex, there are again two possibilities. If $s_l > s_r$, we construct the convex hull of f in $[s_l, s_r]$, i.e., the smallest convex function $H(s) \geqq f(s)$. Our f has a single inflection point and thus H consists of a straight line of slope S and a portion of the graph of f, the two being tangent to each other at a point $(s_0, f(s_0))$. If $s_r = 0$, $s_0 = (1+\mu)^{-1/2}$. The wave connecting s_l and s_r is a shock moving with speed S followed by a suitable rarefaction wave (see Fig. 1a). If, on the other hand, $s_l < s_r$, we construct the concave hull of f and determine the wave structure from its shape (Fig. 1b). For full details, see [10].

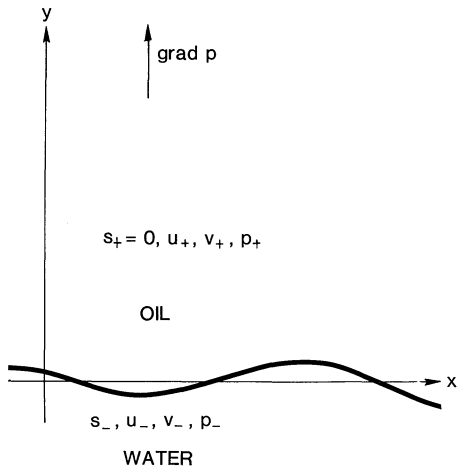

Fig. 2. The perturbation analysis

Consider a physical problem in which water and oil are coexisting in a porous medium without mixing (a description of the physics can be found in [24]). In the region occupied by oil $s=0$, in the region occupied by water $s>0$. The discussion in the preceding paragraph indicates that if water is displacing oil the convex hull of f is used to determine the solution, which consists of a shock followed by rarefaction. If oil is displacing water, the concave hull is used, with analogous conclusions. This construction has been worked out in [24] by physical arguments with no explicit use of condition (E).

Suppose $u \not\equiv 1$, $u>0$, in Eq. (4): the wave speeds are merely scaled by u. If $u<0$, the roles of s_l, s_r, are interchanged in the discussion above: i.e., if the driving velocity changes sign, the displaced fluid becomes the displacing fluid.

Consider a water/oil front coinciding with the x axis, moving steadily in the direction of increasing y (Fig. 2), with water below the x axis and oil above. We wish to consider the stability of the front to small perturbations. The suffix "$-$" refers to quantities defined in the water and the suffix "$+$" to qualities defined in the oil.

In the oil phase $s=s_+=0$. At the front, $s_-=s_0=(1+\mu)^{-1/2}$. The quantity $\lambda(s_0)/\lambda(0)\equiv M$ is called the mobility ratio. Write $p_\pm=P_\pm+p'_\pm$, $s_-=S_-+s'_-$, $v_\pm=V_\pm+v'_\pm$, etc., where the capitals denote unperturbed quantities and the primes denote perturbations. Let $\nabla P_\pm=(0,G_\pm)$. From Eqs. (1b), (1c), we find

$$G_+\lambda(0)=G_-\lambda(s_0), \quad G_+, G_->0,$$
$$P_+=G_+y, \quad P_-=G_-y.$$

Substitution into Eq. (1a) yields, to first order in small quantities,

$$(s'_-)_t+V_-a(S_-)(s'_-)_y=As'_-, a\equiv\frac{df}{ds},$$

where A is a function of S_-. On the front itself $s_-=s_0$, $s'_-=0$, and thus $s'_-\equiv 0$ everywhere.

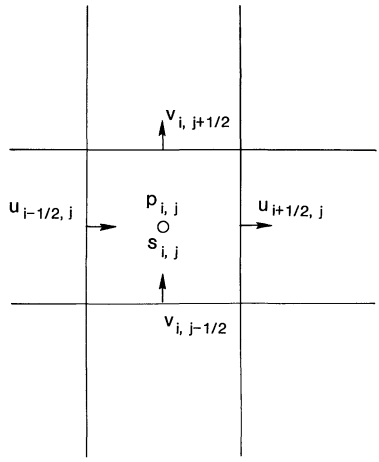

Fig. 3. The computational grid

From this point on, the analysis follows Chouke's argument, published by Saffman and Taylor [23]: From Eqs. (1b), (1c), we find

$$\Delta p'_+ = 0\,, \qquad \nabla\cdot\lambda(S_-)\nabla p'_- = 0$$

with p and v continuous across the front.

Since the saturation s_- below the front forms a rarefaction, the values of s_- approach s_0, and it is natural to look at the simpler problem with $s_- \equiv s_0$, and thus

$$\Delta p'_- = 0\,.$$

We now perturb the front so that it coincides with the curve

$$y = \varepsilon \exp(i\alpha x + \sigma t)\,.$$

An appropriate choice of the forms of p'_-, p'_+ yields

$$p'_\pm = C_\pm e^{\mp\alpha y} \exp(i\alpha x + \sigma t), \qquad C_+, C_- \text{ constants}\,.$$

The boundary conditions yield, after some manipulation,

$$\frac{\sigma}{\alpha}\left(\frac{1}{\lambda(s_0)} + \frac{1}{\lambda(0)}\right) = G_+(M-1), \qquad M = \text{Mobility ratio}\,. \tag{5}$$

For $M > 1$, $\sigma > 0$ for all α and the front is unstable. $M > 1$ if $\mu > 3$. Note that σ is proportional to α, suggesting that the instability is very strong; (compare with the instability of a vortex sheet [18].) There is a continuum of unstable modes.

The Numerical Method

We shall be solving Eqs. (1) by a generalization of the random choice method [13, 3, 4, 10, 15]. The time t is discretized into steps of length k. The quantities p, s, u, v are defined on a staggered grid of mesh length h (Fig. 3), following [17]: p and s are defined at (ih, jh), i, j integers, u is defined at $((i+1/2)h, jh)$, v is defined at

$(ih, (j+1/2)h)$; we write $s(ih, jh) = s_{i,j}$ etc. The boundary conditions (3) are approximated in the obvious manner.

At the beginning of the $(n+1)^{\text{st}}$ time step, it is assumed that the quantities p, s, u, v are known. Equation (1a) is used to calculate $s_{i,j}^{n+1} = s_{i,j}$ at the new time via the random choice method. Equations (1b), (1c) are then used to update p and $\mathbf{u}$.

The one dimensional version of the random choice method can be described as follows: consider the equation

$$s_t + uf_x,\ f = f(s),\ u \text{ given}.$$

At time t the saturation s is assumed known at the points ih, i integer; s is extended to a function constant on the intervals $[(i-1/2)h, (i+1/2)h]$. The resulting initial value problem is solved exactly; the solutions consists of independent Riemann solutions if the CFL condition is satisfied:

$$k \leqq h \max_i (|u| a(s_i, s_{i+1})),$$

where $a(s_i, s_{i+1})$ is the largest velocity which can occur in the solution of the Riemann problem separating s_i and s_{i+1}. We shall assume that this condition is satisfied. The Riemann solutions are then sampled to obtain new values of s. The sampling strategy determines the accuracy of the calculation. Following Colella [9], we use a sampling based on van der Corput sequences. We modify the sequence when necessary to ensure that if ϑ_n, ϑ_{n+1} are successive samples, $-1/2 < \vartheta_n, \vartheta_{n+1} < +1/2$, then $\vartheta_n \cdot \vartheta_{n+1} < 0$. (The reasons are explained in [4].) Furthermore, we also follow Colella's modification of the sampling which allows the values of s to be defined on a fixed spatial grid without staggering; when this is done, it is natural to define u in Eq. (4) at the points $(i+1/2)h$, as will be done in our two dimensional grid.

The natural way to generalize this scheme to two space dimensions is to solve successively the problems

$$s_t + uf_x = 0,\ s_t + vf_y = 0.$$

The flaw in that procedure, pointed out by Colella [9] and Majda [11, 12], lies in the fact that a front which lies diagonally across the grid can be interpreted in one of the directional sweeps as representing water displacing oil and in the other sweep as oil displacing water. Examples of errors which arise in such situations can be found in [11], and the construction which follows is designed to avoid them. Other authors [16, 19] have tried to avoid this difficulty by tracking the fronts.

The general idea is to decide which kind of front is really occurring by using some local two-dimensional information in the one-dimensional sweeps. One can require, without loss of accuracy, that the sampling numbers used in the two directional sweeps be always either both positive or both negative. Assume this has been done. Consider the x-sweep, i.e., the sweep in which the equation being solved is $s_t + uf_x = 0$. For the full Eq. (1a), if $\mathbf{u} \cdot \nabla f < 0$, water is displacing oil and the convex hull of the function f determines the Riemann solution. The opposite is true if if $\mathbf{u} \cdot \nabla f > 0$. Consider the point (i, j), assume $u_{i-1/2,j} > 0$, $v_{i,j-1/2} > 0$, and evaluate the quantities

$$\varrho_1 = u_{i-1/2,j}(f(s_{i,j}) - f(s_{i-1,j})).$$
$$\varrho_2 = v_{i,j-1/2}(f(s_{i,j}) - f(s_{i,j-1})).$$

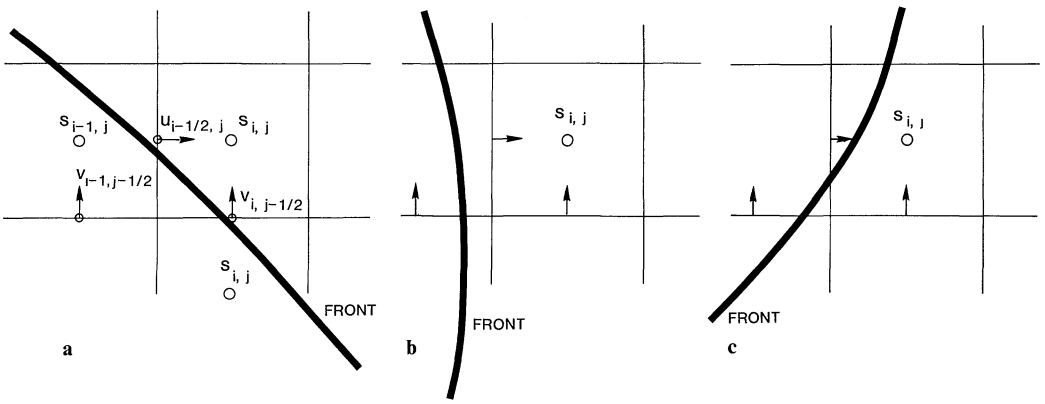

Fig. 4a–c. The front relative to the two-dimensional grid

If $\varrho_1\varrho_2 \geqq 0$, the wave is interpreted in the same way in both the sweep we are performing and in a hypothetical y-sweep, and the x-sweep does not have to be modified. The level lines of s are likely to look as in Fig. 4a or Fig. 4b.

Suppose $\varrho_1\varrho_2 < 0$. The likely level lines look as in Fig. 4c. Evaluate

$$\varrho_2' = v_{i-1,j-1/2}(f(s_{i-1,j}) - f(s_{i-1,j-1})).$$

Let $\varrho = \varrho_1 + \varrho_2'$. If $\varrho \leqq 0$ water is displacing oil, and if $\varrho > 0$, oil is displacing water. If $\varrho \leqq 0$ and $s_{i-1,j} \geqq s_{i,j}$ or $\varrho > 0$ and $s_{i-1,j} \leqq s_{i,j}$ the one dimensional sweep is interpreting the wave correctly. In the other cases the sweep is misinterpreting the nature of the wave and the roles of convex and concave hulls have to be interchanged. This is easily done: one exchanges the roles of s_l, s_r in the Riemann solver and replaces ϑ by $-1/2-\vartheta$ if ϑ is negative, by $1/2-\vartheta$ if ϑ is positive. Note that the one-dimensional sweep may now violate condition (E).

There are three analogous cases to be considered: $u_{i-1/2,j} > 0$, $v_{i,j+1/2} < 0$, then $u_{i+1/2,j} < 0$, $v_{i,j-1/2} > 0$ and finally $u_{i-1/2,j} < 0$, $v_{i,j+1/2} < 0$. Similarly, there are four cases to consider in the y-sweep. Note that the decision process we have just described is not unambiguous: it may well happen that $v_{i,j-1/2} > 0$ but $v_{i,j+1/2} < 0$. Such cases are presumably rare, the corresponding values of v small, and in practice the ambiguity presents no problem.

Finally, given s^{n+1}, the new values of p and $\mathbf{u}$ are found by approximating (1b) by

$$u_{i+1/2,j} = 1/2(\lambda(s_{i+1,j}) + \lambda(s_{i,j}))(p_{i+1,j} - p_{i,j})/h,$$

with a similar expression for v, and approximating $\nabla \cdot \mathbf{u}$ by $D\mathbf{u}$ given by

$$hD\mathbf{u} = u_{i+1/2,j} - u_{i-1/2,j} + v_{i,j+1/2} - v_{i,j-1/2}.$$

The resulting elliptic equation for p is self-consistent in the sense of [2], and thus there are no fictitious sources of s in the domain of integration. Also, the flux of s is conserved, and the natural discrete form of $\nabla \times \nabla p = 0$ is satisfied. This guarantees that we are finding the correct weak solutions of our elliptic equation (see the analysis in [14]). There is no need to worry about the legitimacy of differencing across the front.

Table 1. Vertical velocity in slightly perturbed flows

x	$\mu=2.9$	$\mu=3.1$
1/2	0.3427	0.3245
2/12	0.3427	0.3245
3/12	0.3427	0.3245
4/12	0.3426	0.3249
5/12	0.3422	0.3250
6/12	0.3421	0.3249
7/12	0.3422	0.3246
8/12	0.3426	0.3245
9/12	0.3427	0.3245
10/12	0.3427	0.3245
11/12	0.3427	0.3245

The algebraic equations which arise from Eqs. (1b), (1c) can be solved in a variety of ways (see e.g. [11, 16]). We have obtained satisfactory results by an overrelaxation method with a position dependent relaxation factor.

The method has been successfully tested on several test problems whose solution is known. The calculations presented in the next section also act as a check.

Numerical Results

(a) Growth of Small Perturbations

The linearized stability theory we have presented predicts that for $\mu>3$ small perturbations will grow exponentially. The rate of growth is however relatively small. If we assume $\alpha=\pi$, then σ^{-1}, the e-folding time as predicted by Eq. (5), will be ~ 160 for $\mu=3.1$. Even if we consider the smallest α which can be represented on an economical grid, the corresponding rate of growth is hard to observe in view of the stronger instability we shall discuss in the next section. Note that during the time it takes for a perturbation of small amplitude to grow the front is likely to leave our computational domain. This can be remedied by performing a translation of the form $s'(x,y,t)=s(x,y+Y,t)$, $Y=\text{constant}$, whenever needed.

As a way of exhibiting the linearly unstable modes, consider the initial conditions: $s(x,y,0)=s_0$ for $0\leqq x\leqq 1/3$ and $0\leqq y\leqq 1/2$, $s=s_0$ for $1/3\leqq x\leqq 2/3$ and $0\leqq y\leqq 1/2+1/12$, $s=s_0$ for $2/3\leqq x\leqq 1$ and $0\leqq y\leqq 1/2$, $s=0$ otherwise (this is a front with an extrusion in its middle third). In Table 1 we display the values of the vertical velocity v on the line $y=1/2$ for $\mu=2.9$ and $\mu=3.1$. For $\mu=2.9$ v is smaller in the region of the extrusion, thus reducing its size; the opposite is true for $\mu=3.1$. Thus $\mu=3.0$ is seen to be the dividing point between stable and unstable behavior. Note that the differences in v are in the fourth significant digit.

We have run some initial value problems with s in the water close to s_0 and μ close to 3, $\mu>3$, and observed a growth of perturbations on a time scale compatible with linear theory. We omit the pictures which are singularly undramatic.

```
         9
999999999999999999
```

a *Initial Perturbation*

```
555555555 55555555555
555555555555555555555
555555555555555555555
555555555555555555555
666666666566666666666
666666666566666666666
666666666566666666666
777777777677777777777
777777777677777777777
999999999799999999999
999999999899999999999
999999999999999999999
999999999999999999999
999999999999999999999
```

b $\mu=2.8,\ t=0.90$

```
         5
555555555565555555555
555555555565555555555
666666666666666666666
666666666666666666666
666666666666666666666
666666666666666666666
666666666666666666666
777777777777777777777
777777777777777777777
777777777777777777777
888888888888888888888
888888888888888888888
999999999999999999999
999999999999999999999
999999999999999999999
999999999999999999999
```

c $\mu=2,\ t=0.98$

```
      5      5
         5 55
55555555 5 555555555
55555555    555555555
55555555    565555555
666666655555666666666
666666666655567666666
666666666655567666666
777777777555777777777
777777756666687777777
777777766666697777777
999999996676699999999
999999997797799999999
999999999999999999999
999999999999999999999
999999999999999999999
```

d $\mu=3.0,\ t=1.06$

```
         4
44444          4444444
555554     44 5555555
555554444444 5555555
666664444444456666666
666665555555556666666
666665555556556666666
777776666666667777777
999997777777777999999
999999999999999999999
999999999999999999999
999999999999999999999
```

e $\mu=3.2,\ t=0.96$

```
         4
444444444444444444444
444444444444444444444
555555555555555555555
666666666666666666666
666666666666666666666
666666666666666666666
777777777777777777777
999999999999999999999
999999999999999999999
999999999999999999999
```

f $\mu=3.6,\ t=0.95$

```
         5
         55
         7
         9
         9
444444444494444444444
666666666696666666666
999999999999999999999
999999999999999999999
```

g $\mu=3.7,\ t=0.51$

```
         44
        544
        555
         55
         444
         544
444444444555444444444
555555555655555555555
555555555666555555555
555555555666555555555
555555555666555555555
666655555777555555555
766666666996666666666
999999999999999999999
999999999999999999999
```

h $\mu=4,\ t=0.97$

```
         9
         9
         999
       222  99
         33399
   222     99  999
   2222     939999
   99        99999
    25        9999
    2299994299
     999999999
      9999999
     9999999999
       999999  99
9999   99999   9999999
999999999499999999999
999999999999999999999
999999999999999999999
999999999999999999999
```

i $\mu=20,\ t=1.50$

Fig. 5a–i. Effects of a small perturbation

```
      99999999999
9999999999999999999
```

a *initial perturbation*

```
5555        5555 55555
555555555555555555555
555555555555555555555
666655555555555566666
777766666666666677777
999966667777777699999
999988888888888899999
999999999999999999999
999999999999999999999
999999999999999999999
```

b $\mu=2.7,\ t=0.51$

```
                5
               55
              555
             5566
555555555577555555555
666666666666666666666
777766666966776777777
777777777977777777777
999988888988888899999
999999999999999999999
999999999999999999999
999999999999999999999
```

c $\mu=2.8,\ t=0.66$

```
     55555 555
     55555 5555
      555555555
55   666656665   555
555557777555755555555
666665888688855555888
666666999799966666666
777777999999977777777
999999999999989999999
999999999999999999999
999999999999999999999
999999999999999999999
```

d $\mu=2.9,\ t=0.69$

```
      555    55
     5555    555
      555555555
55   666555666    55
555557776666675555555
666655588666665566666
666666997779966666666
777777999999977777777
999999999999898999999
999999999999999999999
999999999999999999999
999999999999999999999
```

e $\mu=3.0,\ t=0.69$

Fig. 6a–e. Effects of a larger perturbation

(b) Growth of Finite Amplitude Perturbations

In Figs. 5 and 6 we display the flow that arises from the front perturbed as depicted for various values of μ. In each point occuped by water we print the integer $[10s]$, where the square bracket denotes the integer part. When $s=1$, we print 9. This device is similar to the one used by Glimm [15] and is necessary because it has not proved possible to design a contour plotter which gives a good account of the complexity of the flow.

In Fig. 5 the initial perturbation has a very small physical extent. For $\mu<2.8$ the flow is stable in the simplest way: the perturbation simply disappears. For μ between 2.8 and 3.5 we observe a paradoxical effect. An initial extrusion of water becomes an intrusion of oil with a little "foam" in front. The particular structure of the foam is quite likely to be a numerical artifact. The reason for this phenomenon is quite obvious: since x is not convex (see Fig. 1), and s is larger behind the extrusion, the velocity of water is smaller there. If the values of v are not large enough to make up for this effect, oil will intrude. After that intrusion the flow changes very slowly; presumably, if $\mu>3$, the perturbation will grow on a time scale consistent with the linearized theory. When $\mu\cong 3.6$ the paradoxical effect disappears, and for $\mu\geqq 3.6$ we see the rapid growth of a thin finger. The eventual complexity of the flow can be seen in Fig. 5i.

In Fig. 6 the initial perturbation has a larger lateral extent and thus more energy for overcoming the paradoxical effect. Note that the perturbation is growing rapidly even for $\mu = 2.8$, below the critical value of the linearized theory.

The perturbation has a better chance of growing if: (i) its amplitude is increased, (ii) its physical extent is increased, (iii) μ is increased, and (iv) the gradients of s below the front are increased. We have not been able to characterize the successful perturbations in a mathematical reasonable way, nor to relate the finite amplitude catastrophic instability to the linear theory. Clearly, when finite amplitude perturbations are allowed, the larger values of s below the front can affect the front and create a large "eddy" mobility ratio. Note that the main new feature of our numerical method, i.e., the modification of the splitting, has little bearing on the analysis of the early stages of finite amplitude instability in our geometry. The important balance is between the solution of the elliptic Eqs. (1b), (1c) and the properties of the one dimensional Riemann solution. The fingers we are seeing are of the same kind as the ones previously observed by Concus, Glimm, and Lotstedt. For experimental results, see e.g. [14].

The results regarding stability are compatible with those in [13] and [19]: the front is stable for $\mu = 2$ ($M = 0.845$) and dramatically unstable for $\mu = 4$ ($M = 1.105$). A finite amplitude perturbation is needed to generate an instability that can be discerned in a reasonable time. It remains to see whether our amplitudes are comparable with those in [15, 16], since previous authors provide few data around $\mu = 3$. Above $\mu = 4$, the amplitude needed may well be comparable with truncation and round-off error.

One can also display interesting runs in which a small perturbation grows for a while as per the linearized theory and, once some threshold is crossed, begins to grow at a much faster rate. Finally, even when $s = s_0$ below the front, large enough perturbations grow much faster than the linear theory predicts.

Note that the range of mobility ratios in which these phenomena occur is very small: below $M = 0.97$ all perturbations decay both in the linearized mode and in the short run for large perturbations; above $M = 1.06$ our calculation show a catastrophic growth of perturbations whose physical extent is a single mesh cell in a 20×20 grid. As far as we know, ours is the first calculation in which the onset of instability is computed reliably.

(c) Fractalization

It is natural to wonder what happens to the front beyond the onset of instability. A look at Fig. 5i and the much more complex figures which are obtained with a finer grid, as well as the fact that Eqs. (1) are invariant under changes of time and length scales, suggest that the front eventually approximates a fractal set (i.e., a set of non-integer Hausdorff dimension; see e.g. [20]).

To test this conjecture we proceed as follows: At $t = 0$ assume the front is flat, represent it on an $n_1 \times n_1$ grid, and give it a random perturbation. This is easily done by adding to the ϑ's in the random choice method a small random component which is a function of $\mathbf{x}$ and t (such a device was already used in [16]). Turn off the perturbation when the front has changed its length and the instability has set in, and compute up to a time T_1. Suppose that at time T_1 the number of cells which lie on the boundary between water and oil is l_1.

Table 2. Estimates of D

$\mu=28$,	30×30 grid:	$\mu=28$,	40×40 grid:	$\mu=5$,	30×30 grid:	$\mu=5$,	40×40 grid:
	1.33		1.35		1.28		1.25
	1.79		1.35		1.44		0.97
	1.71		1.83		1.33		1.16
	1.01		0.91		1.66		1.89
	0.68		1.54		1.16		1.46
	1.24		1.99		1.38		1.28
average:	1.30		1.48		0.91		1.45
			1.79		1.10		1.44
			1.00		1.33		1.57
		average:	1.44		1.54		1.22
$\mu=10$,	30×30 grid:	$\mu=10$,	40×40 grid:		1.00		1.23
	1.26		1.32		2.08		2.68
	1.36		1.60		1.06		2.86
	1.52		1.36		1.30		1.61
	1.31		0.31		1.46		0.88
	2.27		0.88		1.64		2.03
	1.51		1.45		1.81		2.26
	1.33		1.07		1.49		1.00
	2.35		1.35	average:	1.38		2.75
	1.46		1.33			average:	1.60
average:	1.59		1.85				
			1.21				
		average:	1.25				

Suppose we were to restart the calculation on an $n_2 \times n_2$ grid, and run up to the same time T_1, with $n_2 > n_1$. We would get more detail, and if the number l_2 of boundary points is larger than $l_1 \times (n_2/n_1)$ we have grounds for the belief that the boundary is a fractal set.

Once we reach the time T_1 with the second calculation, we can take the subsquare $0 \leqq x \leqq \beta$, $0 \leqq y \leqq \beta$, $\beta = n_1/n_2$, expand it to fill the whole square and increase the time scale by the factor $1/\beta$. Since the equations are invariant under simultaneous changes of scale in time and space, the resulting configuration could have been obtained by running the initial calculation up to a time T_1/β. (There are some minor differences at the boundaries of the domain which are presumably insignificant; a similar device was used in [6].) Thus we can obtain an estimate of the Hausdorff dimension D of the boundary between oil and water by comparing the results of a single calculation at different times. If l_i is the number of boundary points at time T_i, and l_{i+1} is the number of boundary points at time T_{i+1}, the analysis in [20] shows that the dimension D is approximated by

$$D \sim [\log l_{i+1}/l_i)/\log(T_{i+1}/T_i)] + 1 .$$

We pick $T_i = i\ 20k_0$, where k_0 is a typical time step; in Table 2 we list some computed values of D. The calculations have to be stopped whenever the boundary set fails to fit into our computational domain. The validity of the calculation is not obvious, in particular because it is far from obvious that it is legitimate to compute when the fingers are one mesh width thick, and because it is unclear that the neglected detail at any stage of the computation should not have an effect on what is actually seen. One could speculate that the results in Table 2 suggest a value $D \sim 1.5$ for μ large enough.

```
                                  9
 99   9    9 9         9  9
 999  9999 9 99 99 99 9  9  9 9 9
 99    999 9 99 99 99 9  999 9
999    99999 99 99 99 9  999 9
999     9999 9999999999  999 9
999999999999 99999999999999999
9999999999993999999999999999999
99999999999999999999999999999999
```

$\mu=28$, $t=0.91$, 40×40 *grid (detail)*

Fig. 7. Partial view of a computed front, $\mu=28$

If indeed a process of fractalization does occur, it is obvious that the numerical results obtained from Eqs. (1) in the unstable regime are wholly unreliable and other effects, such as capillary pressure, must be taken into account in practical problems. Finally, in Fig. 7 we show a typical detail of the flow with $\mu=28$. This should be compared with the photographs in [25].

Conclusions

The application of our method to flow problems of direct interest in petroleum reservoir engineering will be presented elsewhere. We would like to emphasize here the broader significance of the results.

We have seen that linearized stability theory for the fronts described by Eqs. (1) predicts a continuum of linearly unstable modes. These modes can be detected if a calculation is done carefully enough, but the important feature of the real instability is the catastrophic growth of localized finite amplitude perturbations which is accompanied by "chaos" in physical space. This situation parallels the transition to turbulence in a boundary layer (see e.g. [5] and the references therein, in particular [22]). In the case of a boundary layer, the unstable modes of the linearized theory are the Tollmien-Schlichting waves, and the analogues of the fingers are the "bursts" connected with the catastrophic stretching of horseshoe vortices. Similar scenarios arise also in the analysis of three dimensional vortex motion [7]. Equations (1) may thus provide a simple model of transition to turbulence in problems where the number of active modes is not restricted by the effects of buoyancy or imposed rotation.

Note. The programs used in the calculations above are available from the author.

Acknowledgment. I would like to thank Professor A. Majda for many illuminating discussions.

References

1. Albright, N., Concus, P., Proskurowski, W.: Numerical solution of the multi-dimensional Buckley-Leverett equations by a sampling method. SPE paper 7681 (1979)
2. Chorin, A.J.: On the convergence of discrete approximations to the Navier-Stokes equations. Math. Comp. **22**, 745–762 (1969)
3. Chorin, A.J.: Random choice solution of hyperbolic systems. J. Comput. Phys. **22**, 517–533 (1976)

4. Chorin, A.J.: Random choice methods, with applications to reacting gas flow. J. Comput. Phys. **25**, 253–272 (1977)
5. Chorin, A.J.: Vortex models and boundary layer instability. SIAM J. Sci. Stat. Comp. **1**, 1–21 (1980)
6. Chorin, A.J.: Estimates of intermittency, spectra, and blow-up in developed turbulence. Commun. Pure Appl. Math. **34**, 853–866 (1981)
7. Chorin, A.J.: The evolution of a turbulent vortex. Commun. Math. Phys. **83**, 517–535 (1982)
8. Chorin, A.J., Marsden, J.E.: A mathematical introduction to fluid mechanics. Berlin, Heidelberg, New York: Springer 1979
9. Colella, P.: Glimm's method for gas dynamics. SIAM J. Sci. Stat. Comp. **3**, 76–110 (1982)
10. Concus, P., Proskurowski, W.: Numerical solution of a non-linear hyperbolic equation by the random choice method. J. Comput. Phys. **30**, 153–166 (1979)
11. Crandall, M., Majda, A.: The method of fractional steps for conservation laws. Numerische Math. **34**, 285–314 (1980)
12. Crandall, M., Majda, A.: Monotone difference approximations to scalar conservation laws. Math. Comp. **34**, 1–14 (1980)
13. Glimm, J.: Solutions in the large for nonlinear hyperbolic systems of conservation laws. Commun. Pure Appl. Math. **18**, 697–715 (1965)
14. Glimm, J., Marchesin, D.: A numerical method for two phase flow with an unstable interface. J. Comp. Phys. **38**, 179–200 (1981)
15. Glimm, J., Marchesin, D., McBryan, O.: Statistical fluid dynamics: unstable fingers. Commun. Math. Phys. **74**, 1–13 (1980)
16. Glimm, J., Marchesin, D., McBryan, O.: Unstable fingers in two phase flow. Commun. Pure Appl. Math. **24**, 53–75 (1981)
17. Harlow, F., Welch, J.: The numerical solution of viscous incompressible flow with a free surface. Phys. Fluids **8**, 2182–2188 (1965)
18. Landau, L., Lifshitz, E.: Fluid mechanics. London: Pergamon 1959
19. Lotstedt, P.: A front tracking method applied to Burgers' equation and two phase porous flow. J. Comput. Phys. **47**, 211–228 (1982)
20. Mandelbrot, B.: Fractals: form, chance and dimension. San Francisco: Freeman 1975
21. Peaceman, D.W.: Fundamentals of numerical reservoir simulation. Amsterdam, New York: Elsevier 1977
22. Rogler, H.L., Reshotko, E.: Disturbances in a boundary layer introduced by a low intensity array of vortices. SIAM J. Appl. Math. **28**, 431–441 (1975)
23. Saffman, P., Taylor, G.: The penetration of a fluid into a porous medium or Hele-Shaw cell containing a more viscous liquid. Proc. R. Soc. A **245**, 312–322 (1958)
24. Scheidegger, A.E.: The physics of flow in porous media. Toronto: University of Toronto Press 1974
25. Wooding, R.A.: Growth of fingers at an unstable interface in a porous medium or Hele-Shaw cell. J. Fluid Mech. **39**, 477–495 (1969)

Communicated by A. Jaffe

Received April 27, 1983; in revised form May 23, 1983